Review

Mechanisms of NO$_2$ Detection in Hybrid Structures Containing Reduced Graphene Oxide: A Review

Sabina Drewniak * [ID]**, Łukasz Drewniak and Tadeusz Pustelny**

Department of Optoelectronics, Faculty of Electrical Engineering, Silesian University of Technology, 44-100 Gliwice, Poland; lukasz.drewniak@polsl.pl (Ł.D.); tadeusz.pustelny@polsl.pl (T.P.)
* Correspondence: sabina.drewniak@polsl.pl

Abstract: The sensitive detection of harmful gases, in particular nitrogen dioxide, is very important for our health and environment protection. Therefore, many papers on sensor materials used for NO$_2$ detection have been published in recent years. Materials based on graphene and reduced graphene oxide deserve special attention, as they exhibit excellent sensor properties compared to the other materials. In this paper, we present the most recent advances in rGO hybrid materials developed for NO$_2$ detection. We discuss their properties and, in particular, the mechanism of their interaction with NO$_2$. We also present current problems occuring in this field.

Keywords: rGO; reduced graphene oxide; NO$_2$; SnO$_2$; SnS$_2$; ZnO; NiO; Fe$_2$O$_3$; CuO$_2$; Polypyrrole; sensing mechanism

1. Introduction—Problems of NO$_2$ Detection

Dynamic urbanization, industrialization and development of agriculture vitally increases pollution of the natural environment. The polluted environment has a negative influence on human health. It causes many medical problems associated with consumption of contaminated food and water and breathing polluted air [1]. Therefore, the control of selected water and air parameters as well as adherence of actual standards set by the health organizations are crucial issues. One of the basic environmental threats is emission of nitrogen dioxide (NO$_2$). NO$_2$ is a highly reactive and toxic gas [2–4]. It is generated through combustion of fossil fuels (heating, power generation, engines in vehicles, etc.) [4], hence, is a serious challenge for the energy and automotive industries [3,5]. At concentrations currently measured in cities of Europe and North America, it causes an increase in symptoms of bronchitis in asthmatic children and reduces lung function growth [6,7], while at concentrations of 150 ppm it could even cause death [7]. Due to these threats, safety standards for NO$_2$ exposures were formulated by many countries and world health organizations. For example, the United States Environmental Protection Agency established the annual exposure limit at 53 ppb [3,8], while the World Health Organization and European Union set it at even 21 ppb [3]. The need for monitoring low concentrations of NO$_2$ in air made the development of NO$_2$ sensors a leading topic of research.

For NO$_2$ detection, various materials have been proposed as sensor layers, e.g., ZnO, WO$_3$, SnO$_2$, Fe$_2$O$_3$, etc. [9–14]. Generally, they exhibit excellent performance in NO$_2$ detection, however, this is mainly at high temperature. High working temperature increases the energy consumption of the sensor, increases a safety hazard, degrades device stability and reduces the operating life. Therefore, there are attempts to replace them by other materials, free from these disadvantages. Realization of this goal is currently the hotspot of research.

2. Graphene and Graphene Oxide as a Gas Sensing Structure

In recent years, special attention has been paid to graphene and graphene oxide [15–19]. An ideal graphene is a one atom thick layer arranged in a two-dimensional honeycomb

lattice, composed of carbon atoms with sp^2 hybridization [20–22]. The two-dimensional structure of graphene causes that it has a zero band gap and acts as a semimetal. It exhibits excellent mechanical, electrical, optical and thermal properties. Due to the huge surface area (~2630 m^{2}g^{-1}), high thermal conductivity (above 3000 W m K^{-1}), high electron mobility at room temperature (~2 × 10^5 cm^2/V·s), carrier density (10^{12}/cm^2) and small resistivity (10^{-6} Ω·cm), it seems to be an ideal candidate for the sensor's layer [20,22]. However, perfect graphene does not have dangling bonds, defects and additional functional groups, which have a strong influence on the gas adsorption [20,23,24]. Moreover, high production cost and low capacity of production methods make the application of pristine graphene still limited [25]. In this respect, derivatives of graphene [20,26], especially graphene oxide and reduced graphene oxides (rGO), are much more attractive. Therefore, the interest in these materials is increasing every year (Figure 1).
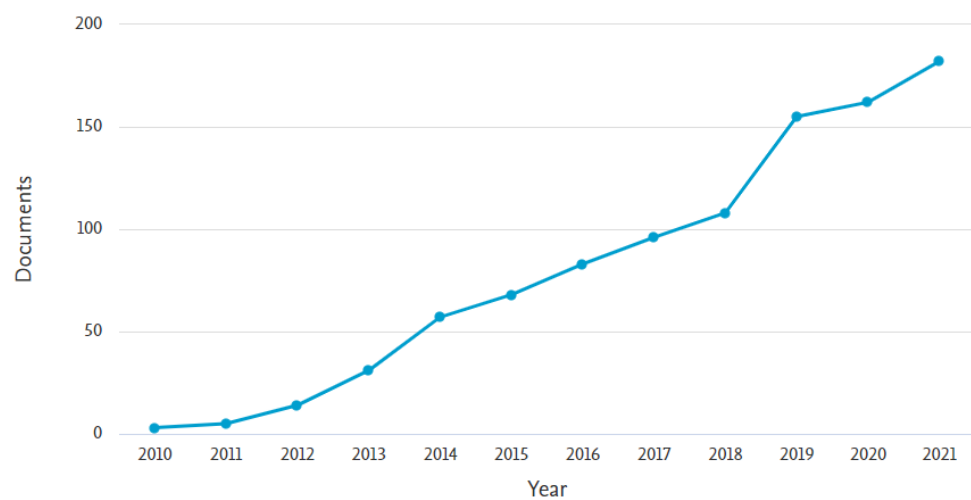

Figure 1. Number of articles per year devoted to the study of sensor properties of graphene oxide and reduced graphene oxide in aspect of sensor applications, prepared based on data from the Scopus database.

However, for sensor applications, rGO is more preferable because of higher conductivity and richer sorption sites compared to graphene oxide.

Reduced graphene oxide is a p-type semiconductor which consist of carbon, oxygen and hydrogen atoms [27,28]. The most common ratio of carbon to oxygen (C/O) is 12:1, although there are also reports where the value of 246:1 is given [29]. Oxygen and hydrogen are attached to the structure in the form of functional groups such as carbonyl (C=O), carboxyl (C-OOH), hydroxyl (C-OH) or epoxy (C-O-C) [8,30,31]. The number of functional groups is determined by (among others) a reduction method [29,32]. The reduction method can affect the response of the sensing structure due to the appearance of additional adsorption sites for gas [2]. For example, rGO fabricated using L-ascorbic acid has a higher degree of oxidation, a smaller amount of functional groups and a higher number of defects than rGO fabricated using hydrazine hydrate [2]. Therefore, the second oxide exhibits higher sensitivity for NO$_2$ detection. Similar research on the influence of the reduction method and graphite precursor on the structure and physicochemical properties of rGO (in terms of the detection of selected gases, including NO$_2$) were also carried out by the authors of this paper and published in [33,34].

The preparation of reduced graphene oxide is realized in three main steps: graphite oxidation, exfoliation of graphite oxide and reduction of graphite oxide sheets (Figure 2).
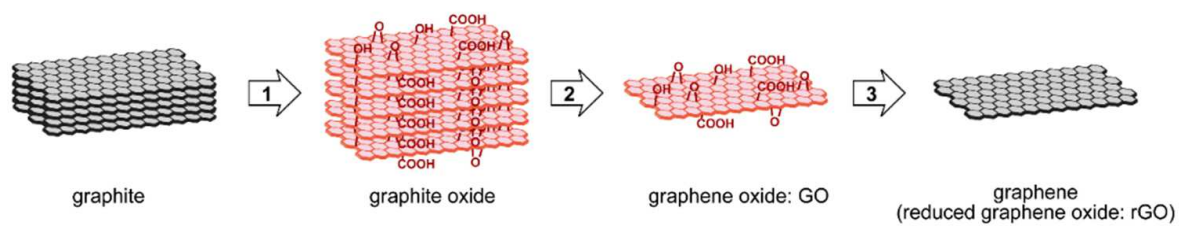
Figure 2. Scheme of fabrication process of reduced graphene oxide; (1) oxidation, (2) exfoliation, (3) reduction. Reprinted from Ref. [35].

In the first step, the graphite precursor is oxidized to the form of graphite oxide [36]. Different methods are used for this purpose. The most known are Hummers', Staudenmaier's, Brodie and Tours' methods [36–40]. During this process, additional oxygen containing functional groups (e.g., epoxy (C-O-C), hydroxyl (OH), carboxyl (R-COOH) and carbonyl (C=O)) are introduced, both to the edges of sheets and to the basal plane [36]. These groups increase the distance between the layers and the hydrophilicity of the layers [29]. In this case, an amount of carbon is from two to four times greater than the oxygen, depending on the preparation method [29]. The structure of graphite oxide consists of carbon atoms with sp^2 and sp^3 hybridization [29]. The carbon atoms are disordered due to attaching to functional groups [29], however, the graphene-like honeycomb lattice is preserved [29]. Obtained graphite oxide is an electrical insulator and is soluble in many solvents, both aqueous and organic [29]. In the next step, graphite oxide is exfoliated into monolayers or few-layered stacks of graphene oxide. This can be achieved by various thermal and mechanical methods [41]. The most common methods are sonicating or stirring in water. The aim of this process is to receive a monolayer (or at most several layers), which is called graphene oxide (GO) [42]. Finally, reduction is carried out. This is one of the most important processes, because it has a significant influence on the quality of produced material [29,40,43]. It determines how the structure of produced material is similar to pristine graphene. The reduction process removes functional groups [29,44] and defects in atomic-scale lattice [29], and recovers the conjugated network of graphitic lattice, as well [29]. The reduction process could be performed simultaneously with the exfoliation process [41] or as a separate process, e.g., using reductants, such as sodium borohydride, hydrazine, formaldehyde, sodium hydroxide and L-ascorbic acid [42]. The final product is called reduced graphene oxide (rGO) [37] or chemically modified graphene [41] (Figure 2). There are many methods to reducing graphene oxide. They can be classified into three main categories: chemical reduction, thermal reduction and electrochemical reduction. Depending on the method used, the obtained material may differ in properties. The main parameters used for estimating the effect of reduction are C/O ratio, structural defects and electrical conductivity [45]. Generally, chemical reduction produced rGO with a low surface area and low conductivity compared to the GO precursor. Thermal reduction produced rGO with a high surface area (close to that of pristine graphene) and with many structural imperfections (vacancies, voids and mechanical stress). Electrochemical reduction produced rGO the most similar to pristine graphene in terms of structure. The choice of the reduction method depends on the planned use of the rGO. In sensor applications, the electrochemical reduction is the most often used method, despite its toxicity. However, in our own research, we use the thermal reduction instead of chemical reduction because it is environmentally friendly and the reduction is performed simultaneously with exfoliation processes. Moreover, the degree of reduction process can be easily controlled by temperature [32].

SEM images of graphite, graphene oxide and reduced graphene oxide are shown in Figure 3.
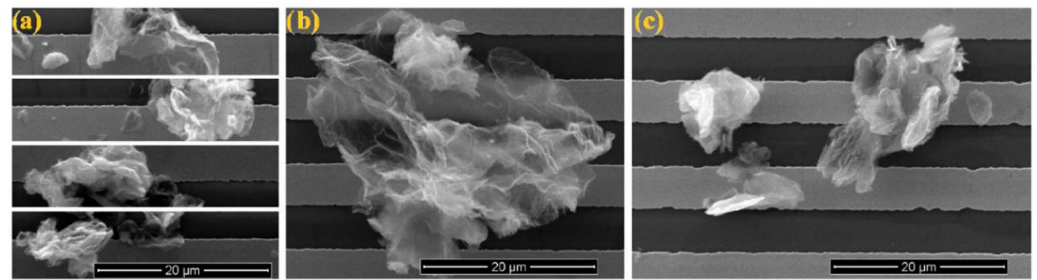
Figure 3. SEM images of reduced graphene oxide. (**a**) modified Hummers' method and modified Tour's method: (**b**) cloud-like particles and (**c**) compact particles. Reprinted from Ref. [34].

Despite the fact that reduced graphene oxide has an extremely large active area [46] and richer sorption sites than graphene and graphene oxide [47], it still has unsatisfactory gas sensitivity [46,48] and selectivity [8]. Therefore, to improve its properties, there are attempts to combine it with other materials used as receptor's layers, e.g., semiconductors [8,49], semiconductor metal oxides (SnO_2, ZnO, NiO) [46], conductive polymers [50], etc. In such structures, rGO is a doping material while the other components are the base materials. Usually, rGO concentration does not exceed a few percent. It is interesting that the literature uses various names for these types of materials, which can be confusing. The most often used names are: hybrid, nanohybrid, composite or nanocomposite. In our opinion, these materials are hybrids because they meet the definition of the hybrid material (have new properties/functions which component materials did not possess, or interpenetrated components are on a scale of less than 1 μm) [51]. Therefore, in the further part of this paper, we will call these materials hybrids. The main advantage of rGO hybrids is the elimination of the disadvantages of the particular components. Generally, rGO hybrids are characterized by: (i) low working temperature, (ii) high electrical conductivity and (iii) huge active sites.

In this paper, we present the most recent advances in rGO hybrid materials developed for NO_2 detection. We discuss the properties of these materials and, especially, the mechanism of their interaction with NO_2. Understanding the processes taking place on the surface of rGO sensors exposed to NO_2 in air is a key issue in developing sensitive and thermodynamically stable sensor layers. In this paper, we also present current problems occurring in this field. In our considerations, we will focus on resistance sensors, in which the resistance varies with the presence of an analyte (NO_2). A simplified principle of operation of such a sensor is presented in Section 3.

3. Principle of Operation of a Semiconductor Resistance Sensor

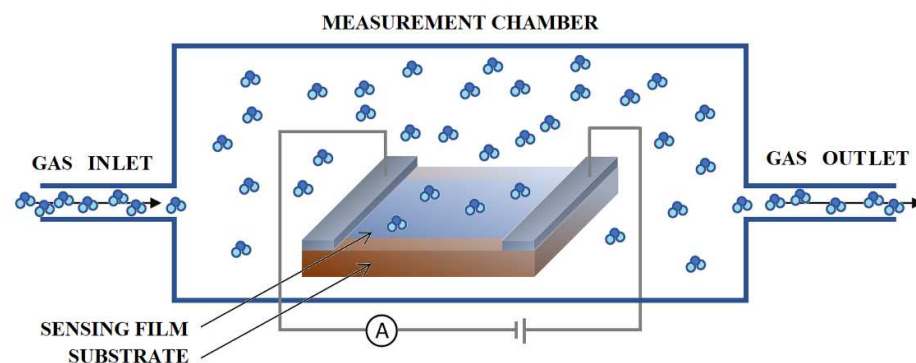The simplified principle of operation of a n-type semiconductor resistance sensor is shown in Figure 4.

Figure 4. The simplified principle of operation of a n-type semiconductor resistance sensor.

A voltage is applied to the sensor which causes the current flow in the electric circuit. When gas appears, the gas molecules interact with the semiconductor surface to form chemical or Van der Walls bonds between the gas molecules and the adsorbent material. This process is called chemisorption and physisorption, respectively. Depending on the type of gas (reducing or oxidizing), electrons can be transferred from the surface of the sensor to the adsorbed gas molecules or in the opposite direction. This causes a change in the concentration of electric charge in the subsurface layer. The change in the concentration of electric charge in this area causes a change in the bands bending near the surface of the semiconductor. As a result, the resistance of the sensitive layer changes. The change in the semiconductor resistance causes a change in the electric current. By measuring the electric current (I) in the electric circuit and knowing the voltage across the sensor (V), the sensor resistance can be easily determined using the Ohm's equation: $R = V/I$. Since the absolute change in resistance does not say much about the sensitivity of the sensor, the relative change in resistance is determined using one of the following equations: $S = \frac{R_g - R_r}{R_r}$, $S = \frac{R_r}{R_g}$, $S = \frac{R_g}{R_r}$, where R_r and R_g are the sensor resistance in reference to atmosphere and in investigated gas, respectively. The higher the sensitivity of the sensor layer, the higher the parameter S. If the test gas and the reference gas are dosed sequentially in the measuring chamber, periodic peaks will be visible on the diagram of sensor signals over time, as shown in Figure 5. Since the operating temperature of a gas sensor determines its sensitivity, the sensor is heated to the temperature where its sensitivity is the highest.
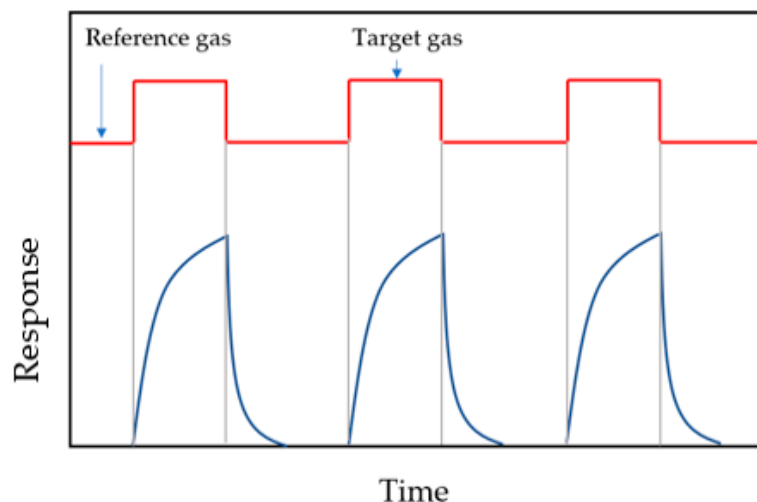

Figure 5. Illustration of the response signal of a semiconductor resistance sensor to the target gas.

4. Mechanism of NO$_2$ Detection in rGO Hybrid Materials

The most often reported rGO hybrid materials for NO$_2$ detection are: rGO/SnO$_2$, rGO/SnS$_2$, rGO/ZnO, rGO/ZnO/NiO, rGO/Fe$_2$O$_3$ and rGO/polypropyrolle/CuO$_2$. We describe the properties of these materials in separate subsections. In each case, the sensing mechanism is identified and discussed.

4.1. Reduced Graphene Oxide and Tin (IV) Oxide (rGO/SnO$_2$)

Tin (IV) oxide (SnO$_2$) is a n-type semiconductor [5,50,52] with a good physical and chemical stability [53]. It belongs to non-toxic [53] and inexpensive material [53]. It has low surface area [50], high working temperature [50,53] and low electrical conductivity at room temperature [52]. In contact with NO$_2$, its conductivity decreases [53]. The combination of rGO nanoflakes with micro- and nanoparticles of SnO$_2$ causes a reduction in SnO$_2$ grains and limitation of its aggregation [53]. SEM images of rGO and rGO/SnO$_2$ with various concentrations of rGO are shown in Figure 6.
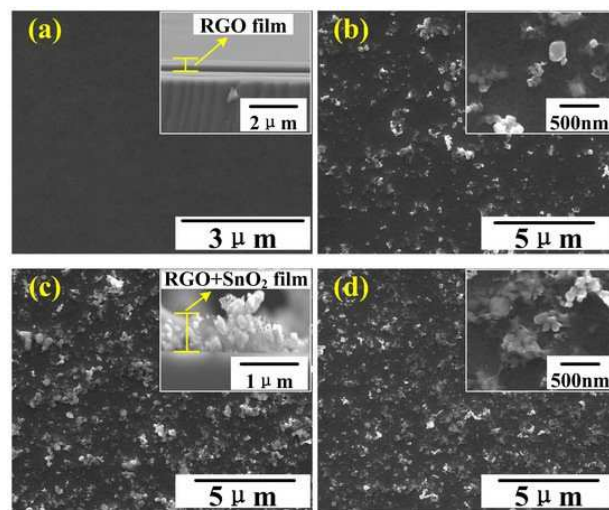
Figure 6. SEM images of: rGO (**a**), 9.7% rGO/SnO$_2$ (**b**), 5.1% rGO/SnO$_2$ (**c**) and 2.6% rGO/SnO$_2$ (**d**). Reprinted from Ref. [54]. The mixture of rGO and SnO$_2$ was prepared using the air brush method.

The surface area of rGO/SnO$_2$ is much greater than both materials separately [50] and contains a high density of interface states. Its resistance is smaller than pure SnO$_2$ [50,53]. In the aspect of NO$_2$ detection, rGO/SnO$_2$ exhibits enhanced response level, shorter recovery time and long-term stability [50]. Its sensitivity strongly depends on the rGO concentration [50,55] and, generally, increases with increasing rGO concentration [50]. The rGO concentration also determines the conductivity type of the rGO/SnO$_2$ hybrid [56]. The improved properties of the rGO/SnO$_2$ hybrid are associated with the following reasons [50,56]:

1. reduced graphene oxide has a favored porosity and broad specific surface area that provides more active sites for NO$_2$ adsorption;
2. high carrier mobility of rGO allows it to increase an electron transport between NO$_2$ molecules and conduction band of rGO/SnO$_2$ hybrid;
3. p–n heterojunctions may enhance the NO$_2$ adsorption due to more highly active sites, and it can cause a broader electron depletion layer.

The schematic band diagram of SnO$_2$ and rGO before contact, rGO/SnO$_2$ heterojunction in air and in NO$_2$, as well as the mechanism of rGO/SnO$_2$ interaction with NO$_2$ are shown in Figure 7.
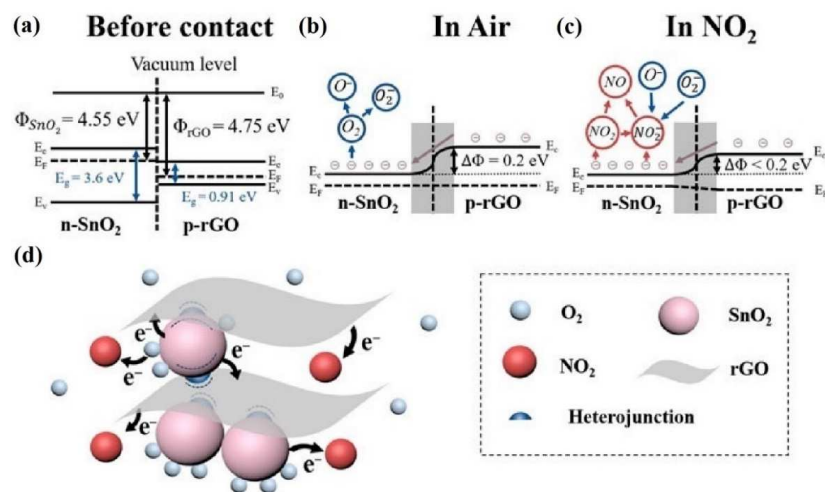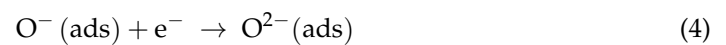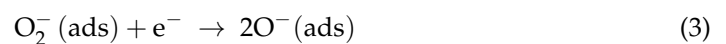

Figure 7. Band diagram of n-type SnO$_2$ and p-type rGO before contact (**a**), rGO/SnO$_2$ heterojunction in air (**b**) and in NO$_2$ (**c**), possible NO$_2$ gas-sensing mechanism of rGO/SnO$_2$ (**d**). Reprinted from Ref. [57].

The introduction of rGO to SnO_2 causes a formation of the p–n heterojunction. Due to the difference in Fermi levels in both materials, electrons flow from SnO_2 to rGO. This causes a formation of the depletion layer at the interface of both materials (there is an increase in electron concentration in the rGO and an increase in hole concentration in the SnO_2). When rGO/SnO_2 is exposed to air, oxygen is absorbed from the air on the rGO/SnO_2 surface (Equation (1)) [56].

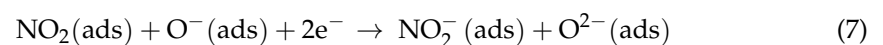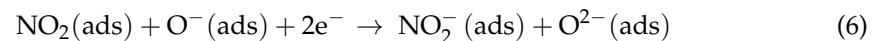$$O_2\,(gas) \;\rightarrow\; O_2(ads) \tag{1}$$

Next, electrons are transferred from the conduction band of the rGO/SnO_2 to oxygen resulting in the formation of negative oxygen ions according to the following reactions [56]:

$$O_2\,(ads) + e^- \;\rightarrow\; O_2^-\,(ads) \tag{2}$$

$$O_2^-\,(ads) + e^- \;\rightarrow\; 2O^-\,(ads) \tag{3}$$

$$O^-\,(ads) + e^- \;\rightarrow\; O^{2-}\,(ads) \tag{4}$$

This causes an increase in the width of the depletion layer and, as a result, the increase in structure resistance. When NO_2 appears, it is adsorbed on the rGO/SnO_2 surface (Equation (5)).

$$NO_2\,(gas) \;\rightarrow\; NO_2(ads) \tag{5}$$

Next, it reacts with both the negative oxygen ions O^- and electrons from the layer, according to the following reactions:

$$NO_2(ads) + O^-(ads) + 2e^- \;\rightarrow\; NO_2^-\,(ads) + O^{2-}(ads) \tag{6}$$

$$NO_2(ads) + O^-(ads) + 2e^- \;\rightarrow\; NO_2^-\,(ads) + O^{2-}(ads) \tag{7}$$

This process leads to a further increase in the depletion layer and increase in the sensor's resistance.

4.2. Reduced Graphene Oxide and Tin (IV) Sulfide (rGO/SnS_2)

Tin (IV) sulfide (SnS_2) is a n-type semiconductor [8] which exhibits poor sensor properties for NO_2 detection at room temperature [49]. At this temperature, its resistance is too high to be measured [8,49]. Although it decreases with increasing working temperature, the probability of its oxidation to SnO_2 increases, as well. The combination of rGO nanoflakes with SnS_2 microstructure (Figure 8) decreases the sensor working temperature. For example, for undoped SnS_2, the working temperature equals 200 °C while for 1.9% rGO/SnS_2, it drops to 25 °C.

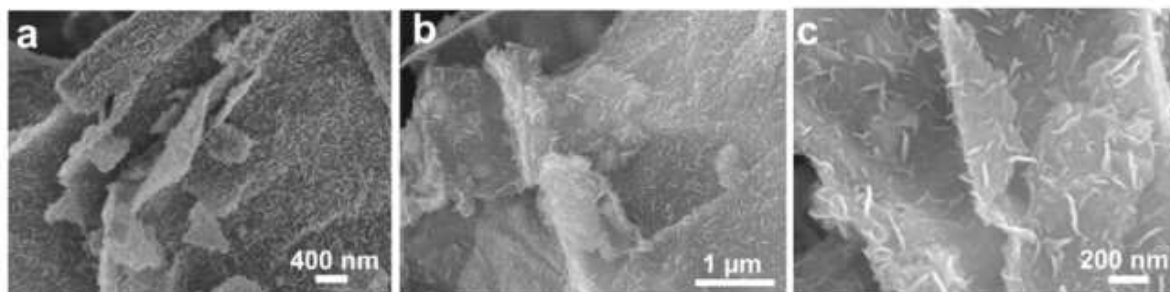**Figure 8.** FESEM image of: rGO/Sn (**a**), rGO/SnS2 with different magnification (**b**) and (**c**), part of the figure. Reprinted from Ref. [58].

However, an increase in rGO concentration has a negative influence on the sensitivity of the hybrid. For example, for a structure with concentrations of 0.8% rGO (Figure 9), a clear response is observed, while for a structure with concentrations of 1% of rGO, it

decreases several dozen times. Increasing rGO concentration also causes deterioration of the response and recovery time and changes the type of hybrid conductivity from n to p [49].
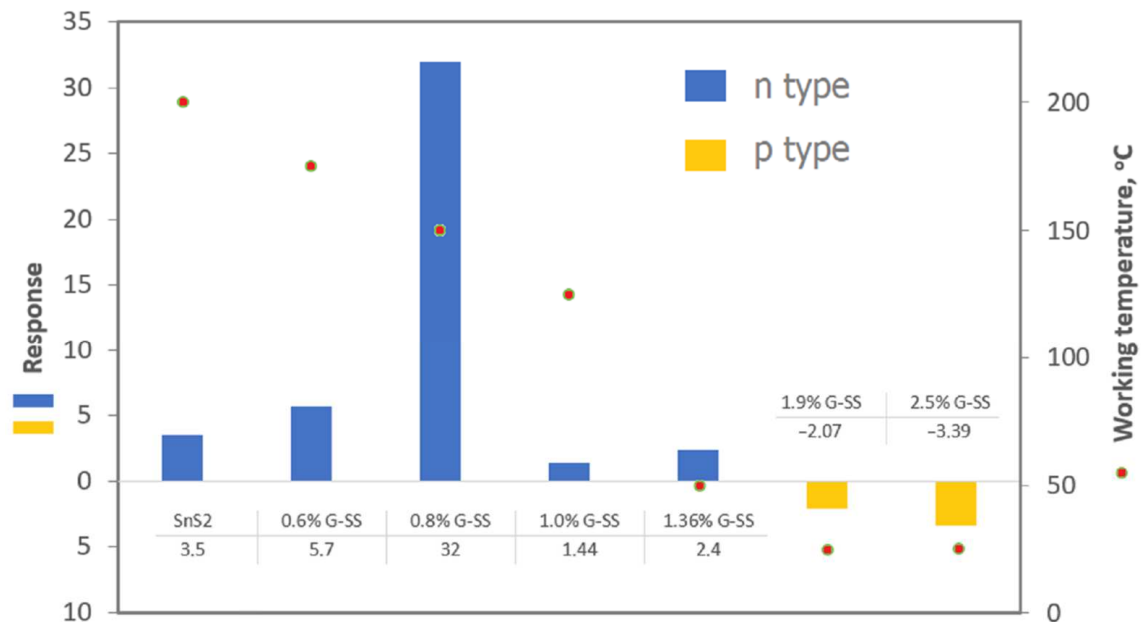

Figure 9. Comparison of sensing response and working temperature among SnS_2 and G-SS (rGO/SnS_2) [49].

The surface area of rGO/SnS_2 is greater than both materials separately [49]. The combination of rGO with SnS_2 causes the formation of C=C, C-O and C-S bonds. The presence of C-S bonds causes vacancies in the structure which facilitate the excitation of electrons into the conduction band. Furthermore, such vacancies are additional active centers for NO_2 adsorption [49].

When SnS_2 is combined with rGO, electrons are transferred from rGO to SnS_2 and the depletion region is formed at the interface of both materials (there is an increase in electron concentration in the SnS_2 and increase in hole concentration in the rGO) [59]. This creates an electrostatic field which, as a consequence, leads to a reduction in activation energy for adsorption/desorption of the target molecules. When the structure is exposed to NO_2, electrons are ejected from rGO/SnS_2. This leads to the reduction in the electron-depletion region in SnS_2 and an increase in the hole-depletion region in the rGO.

4.3. Reduced Graphene Oxide and Zinc Oxide (rGO/ZnO)

Zinc oxide (ZnO) is a n-type semiconductor [46,60,61], which is characterized by good temperature and chemical stability [62,63]. It exhibits poor conductivity at room temperature, therefore, it is used at high temperature (150–450 °C) [60,62,64]. The combination of rGO nanoflakes with ZnO nanoparticles improved its conductivity, provided more active sites to absorb NO_2 molecules and reduced working temperature to room temperature [46,62]. The changes in the rGO/ZnO resistance due to the NO_2 are greater than that of pure ZnO [62,63]. The rGO/ZnO hybrid can be a n-type [62] or p-type [60] semiconductor, depending on the fabrication method. Authors [46] note that the combination of rGO and ZnO effectively prevents the agglomeration of ZnO and also prevents stacking between sheets, which increases the specific surface area. The SEM image of the rGO/ZnO hybrid is shown in Figure 10.
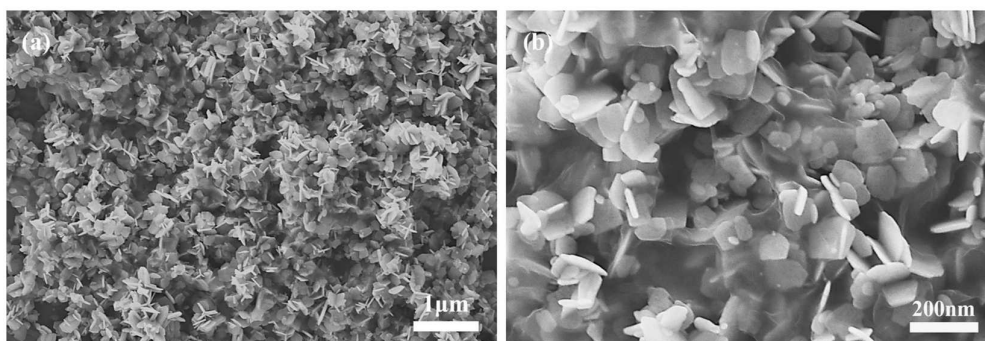
Figure 10. SEM images of rGO/ZnO_{1-x} composites: (**a**) low and (**b**) high magnification. Reprinted from Ref. [64].

The sensor mechanism of rGO/ZnO interaction with NO_2 is similar to the mechanism of pure ZnO [10,62]. In contact with air, oxygen is adsorbed on the surface of the receptor layer according to Equation (8).

$$O_2\,(gas)\ \rightarrow\ O_2(ads) \tag{8}$$

Oxygen takes a free electron from ZnO and becomes an anion (Equation (2)). When NO_2 appears, NO_2 molecules are adsorbed on the rGO/ZnO layer according to reaction 5. The adsorbed NO_2 reacts with a free electron from ZnO forming NO_2^- ions (Equation (7)). NO_2 also reacts with the previously formed oxygen ions and with a free electron from ZnO, forming NO_3^- ions (Equation (9)). Both of these reactions consume free electrons, which causes a decrease in conductivity and, thus, an increase in resistance. Figure 11 shows the band diagram of ZnO and rGO (a) and the possible gas sensing mechanisms of rGO/ZnO nanocomposite in air (b) and in NO_2 (c).
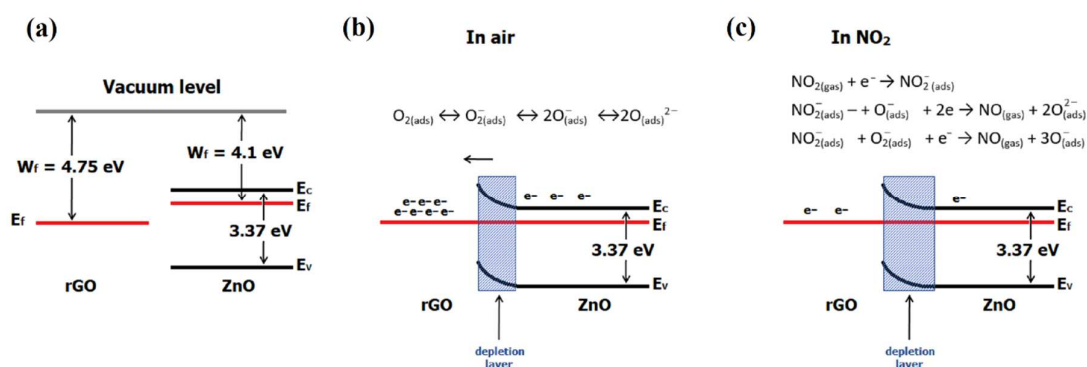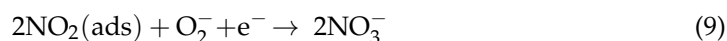
$$2NO_2(ads) + O_2^- + e^- \rightarrow\ 2NO_3^- \tag{9}$$

Figure 11. Band diagram of ZnO and rGO (**a**), possible mechanism of rGO/ZnO in air (**b**) and in NO_2 (**c**).

4.4. Reduced Graphene Oxide, Nickel Oxide and Zinc Oxide (rGO/NiO/ZnO)

In the literature, there are also attempts to combine rGO nanoflakes with several metal oxides nanocomposites. For example, the authors of [61] proposed a concept of combination of rGO with NiO and ZnO. Such a combination allows a layer to be obtained with higher sensitivity (defined as R_{gas}/R_{air}) than for pure ZnO (Figure 12a) and also for the NiO/ZnO composite (Figure 12b,c). As mentioned earlier, ZnO is a n-type semiconductor while rGO is a p-type semiconductor. Nickel oxide is a p-type semiconductor [61] which has high working temperature and poor selectivity [65]. Combining rGO with ZnO/NiO obtains a material similar to a n-type semiconductor. The mechanism of NO_2 detection in rGO/ NiO/ZnO nanocomposites is as follows.
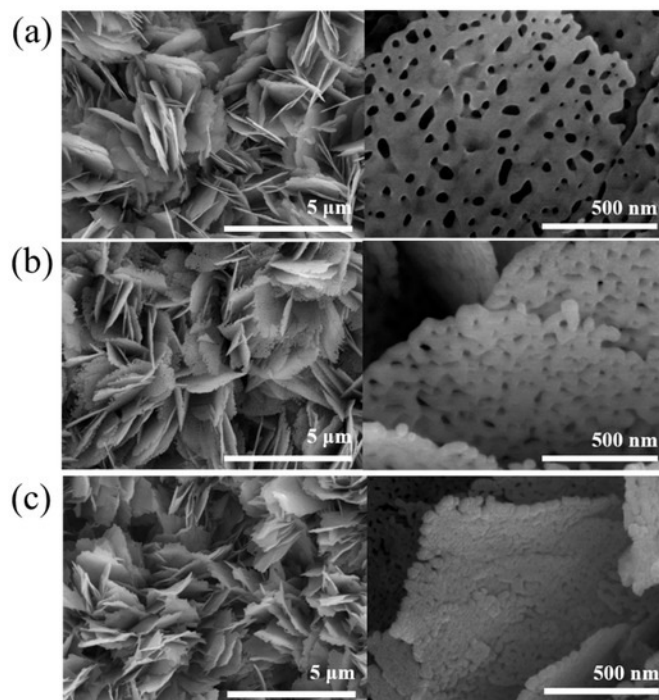
Figure 12. SEM images of pristine porous ZnO nanosheets (**a**) and porous ZnO/NiO composite nanosheets (**b**) and (**c**). Reprinted from Ref. [66].

When ZnO is combined with NiO, electrons flow from the ZnO layer to the NiO layer until the Fermi levels align. This creates an electron-depleted layer on the ZnO side and a hole-depleted layer on the NiO side (Figure 13). When the NiO/ZnO layer adsorbs nitrogen dioxide, it will donate electrons, causing deeper depletion on the ZnO side. At the same time, electrons from NiO will flow to NO_2, which will increase the concentration of holes on the NiO side. As a result, an increase in the response is observed [61]. Reduced graphene oxide nanoflakes in the NiO/ZnO micro- and nanostructure is responsible for the acceleration of electron transfer. This is related to the velocity of adsorption/desorption of the gas and the reactions between the gas and the receptor material [61]. Moreover, rGO provides many additional active sites [61].

4.5. Reduced Graphene Oxide and Iron (III) Oxide (rGO/Fe₂O₃)

Iron (III) oxide (Fe_2O_3) is a n-type semiconductor [67] which is characterized by high electron mobility and chemical stability [68]. It exhibits poor sensitivity to NO_2 detection at room temperatures. The combination of rGO nanoflakes and Fe_2O_3 nanoparticles allows a material similar to a p-type semiconductor to be obtained, which is more sensitive for NO_2 than both materials separately [67]. The SEM image of GO/Fe_2O_3 is shown in Figure 14.

Combination of Fe_2O_3 grains and rGO causes a formation of a heterojunction [67] (Figure 15) in which electrons are transferred from rGO to Fe_2O_3 [67]. rGo/Fe_2O_3 exhibits additional active sites (defects and/or oxygen functional groups) which improve the sensitivity [68]. Reduced graphene oxide, due to its excellent conductivity, can increase the conductivity of the structure [68]. When the structure is exposed in air, oxygen is adsorbed on the surface of rGO/Fe_2O_3 in the forms of O_2^-, O^{2-} and O^- ions [48]. These ions react with NO_2 molecules in the surrounding atmosphere (10) [67] (Figure 16) and, as a result, an unbalanced negative charge is formed on the Fe_2O_3 surface. To neutralize this charge, electrons from the rGO are transferred. This generates holes in the graphene oxide [67] and, finally, causes a reduction in the structure resistance [67].

$$2NO_2(gas) + O_2^- \, ads + e^- \rightarrow \ 2NO_3^- \, (ads) \tag{10}$$
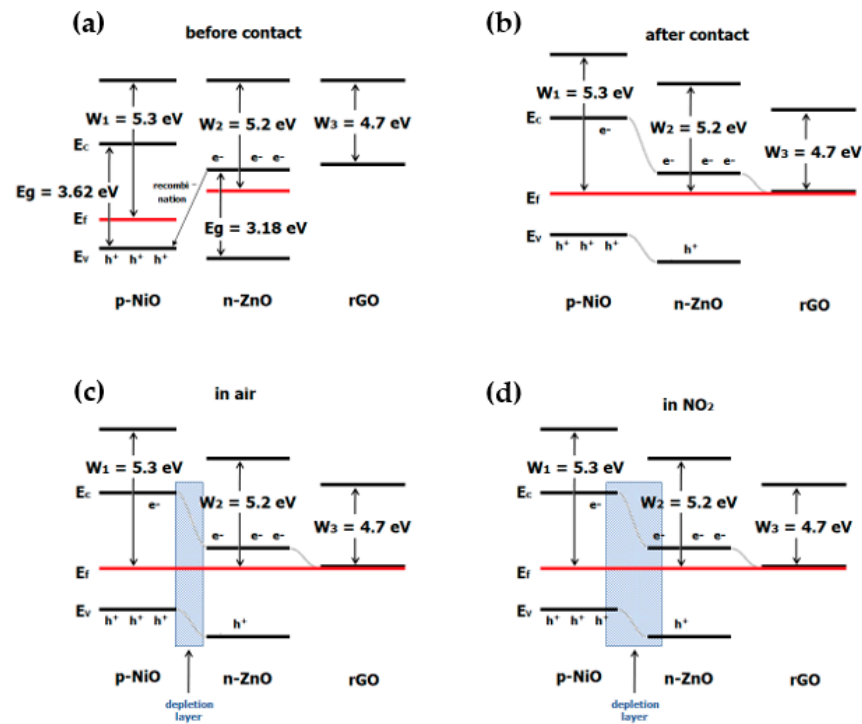
Figure 13. Band diagram of NiO/ZnO before (**a**) and after contact (**b**) and diagrams of gas adsorption on rGO/NiO/ZnO in air (**c**) and in NO$_2$ (**d**).
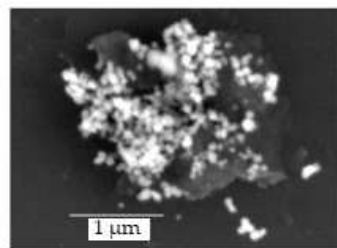

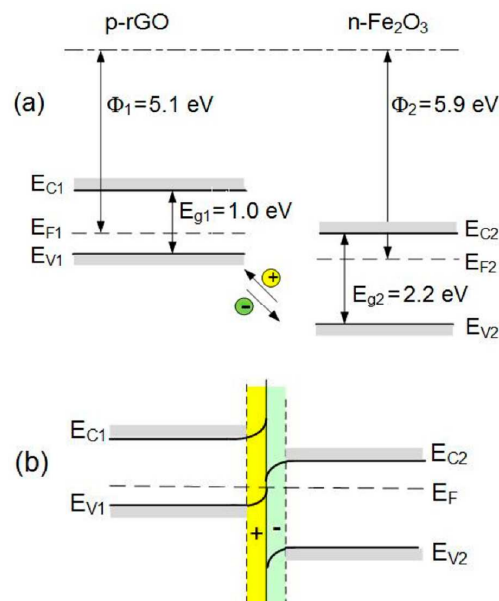**Figure 14.** SEM image of GO/Fe$_2$O$_3$ structure. Reprinted from Ref. [67].

Figure 15. Band diagram of rGO and Fe$_2$O$_3$ before (**a**) and after contact (**b**). Reprinted from Ref. [67].
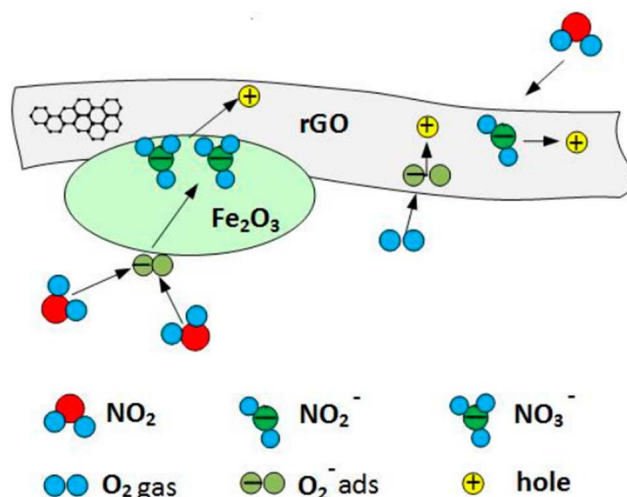
Figure 16. Possible NO_2 gas-sensing mechanism of rGO/Fe_2O_3. Reprinted from Ref. [67].

4.6. Reduced Graphene Oxide, Polypyrrole and Copper (I) Oxide (rGO/PPy/Cu_2O)

Polypyrrole (Figure 17a) is a p-type semiconductor characterized by high chemical stability, high conductivity, redox reversibility, simple preparation and low cost [69]. Therefore, polypyrrole nanostructures are a promising candidate for sensor application. Polypyrrole in combination with rGO (Figure 17b–f) prevents the accumulation/fusion of graphene sheets thanks to electrostatic repulsion between polypyrrole nanoparticles [69]. Additionally, it can enlarge the specific surface area, increase active sites and enhance the adsorption capacity of rGO, improving the affinity for gas [69].
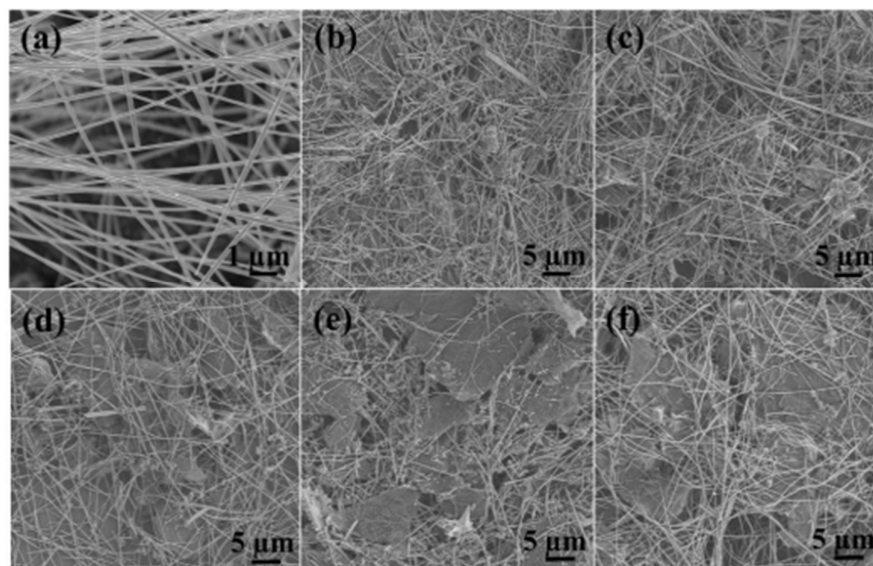
Figure 17. SEM images of PPy (polypyrrole)/Cu_2O nanowires hydrothermally prepared at 120 °C (**a**), rGO/PPy/Cu_2O after high-temperature reduction with mass ratio: 0.08 (**b**), 0.1 (**c**), 0.12 (**d**), 0.15 (**e**) and 0.2 (**f**). Reprinted from Ref. [69].

Copper (I) oxide (Cu_2O) is also a p-type semiconductor which is characterized by low cost, ease of synthesis and stability [70]. Cu_2O have been widely studied for sensing applications in papers [69,71–76]. In combination with rGO, Cu_2O, such as polypyrrole, can enlarge the specific surface area, increase active sites and enhance the adsorption capacity of rGO, improving the affinity for gas [69]. Moreover, Cu_2O can prevent the restacking of graphene sheets and overcome inferior gas selectivity of graphene.

In the case of NO_2 detection, the combination of $rGO/PPy/Cu_2O$ exhibits better NO_2 sensing performance than PPy/Cu_2O composite [69]. When $rGO/Cu_2O/PPy$ composite is exposed in air, oxygen is adsorbed on its surface in the form of O_2^- ions:

$$O_2(gas) + e^- \rightarrow O_2^-(ads) \tag{11}$$

After the introduction of nitrogen dioxide, the NO_2 molecules are trapping electrons from the hybrid material according to reaction (12) and from the oxygen ions (reaction (13)):

$$NO_2(gas) + e^- \rightarrow NO_2^-(ads) \tag{12}$$

$$NO_2(gas) + O_2^- + 2e^- \rightarrow NO_2^-(ads) + 2O^- \tag{13}$$
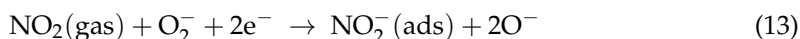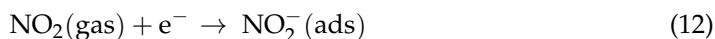
As a consequence, the concentration of holes increases in the hybrid material [69]. The high hole mobility of polypyrrole and graphene flakes favors carrier transport and migration to the electrode. Rapidly reducing the electron concentration and increasing the hole concentration reduces the sensor resistance. The schematic diagram of the sensing mechanism of $rGO/PPy(polypyrrole)/Cu_2O$ is shown in Figure 18.
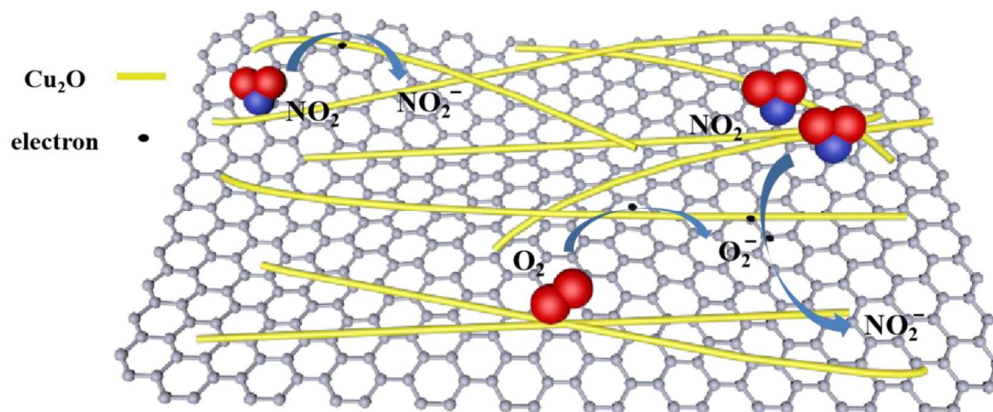

Figure 18. Possible NO_2 gas-sensing mechanism of $rGO/PPy/Cu_2O$. Reprinted from Ref. [44].

In Table 1, we summarize and compare the NO_2 sensing performance of the discussed rGO-based hybrids.

Table 1. Summary of rGO-based hybrids used for NO_2 detection and their performance characteristics.

Hybrid	Temperature (°C)	Concentration of NO_2 (ppm)	Sensitivity	Equation of Sensitivity	Reaction/ Regeneration Time (s)	Ref.
rGO/SnO_2	55	100	1.079	$S = R_{air}/R_{gas}$	-/373	[53]
rGO/SnS_2	80	11.9	56.8%	$S = 100\% \cdot \frac{R_{gas}-R_{air}}{R_{air}}$	360/3180	[59]
rGO/ZnO	RT	1	2.07	$S = R_{gas}/R_{air}$	150/55	[62]
$rGO/NiO/ZnO$	140	2	80.1	$S = R_{gas}/R_{air}$	39/16	[66]
rGO/Fe_2O_3	RT	5	3.86	$S = R_{air}/R_{gas}$	76/946	[48]
$rGO/PPy/Cu_2O$	25	50	42.5%	$S = 100\% \cdot \frac{R_{gas}-R_{air}}{R_{air}}$	-/~200 [1]	[69]

[1] under auxiliary irradiations of an ultraviolet lamp.

5. Remarks on WBS–rGO Hybrid Sensor Structures

The qualitative analysis of the influence of the reduced graphene oxide on the sensor properties of the discussed semiconductors (in particular, oxide semiconductors), in terms of their interaction with NO_2 in air must take into account the fact that they were technologically obtained in the form of nanostructures with a highly developed surface.

Inorganic semiconductor nanostructures (WBS) with a wide band gap ($\Delta Eg > 2$ eV), at room temperature, have a relatively low concentration of free electrons in the conduction

band. They are characterized by slow reaction kinetics: semiconductor–gas analyte (NO_2). Therefore, the amount of electrons available for the effective charge transfer between the adsorbed gas molecules and the surface of the active layer is usually insufficient for its observation in the form of electrical signal. Generally, there are several ways to increase the concentration of electric charge in the conduction band, such as increasing temperature, reducing the bandgap of the semiconductor by introducing defects and impurities, lighting, etc. These kinds of problems and effects were discussed in detail in [10]. In particular, an increase in temperature above 100 °C not only increases the carrier density in the conduction band, but also reduces the effect of humidity on the sensitivity of detected gases (as water molecules adsorbed on the receptor material are heated and evaporated). The increase in temperature improves the sensor's operation. The maximum response is usually at about 200 °C. Above this temperature, the response decreases (resistance increases) due to the sharp increase in the desorption rate of the analyte from the sensor surface. Heating also increases the energy consumption of the gas sensor.

The physical and chemical properties of these semiconductor nanostructures are largely determined by the specific surface area, electronic properties of this surface and the density of interface states in the bandgap of semiconductor.

Electrons from the conduction band, located in the interface states, create an unbalanced electric charge which increases the depletion region. For this reason, the sensitivity of such nanostructures on the oxidizing gases (including NO_2) at low (room) temperatures is low. The interactions of NO_2 with semiconductor structures are relatively weak and exhibit mainly a chemical nature, hardly reversible. The so-called "detoxification process" by treating the structure with air or nitrogen (NO_2-free), at room temperatures, is very slow (it can take tens or event hundreds of minutes). To reduce this time, the structure temperature is increased to 400 K or even more. However, usually, after these processes, the electrical resistance of the structure does not return to its initial value.

The rGO micro- and nanoflakes are characterized by p-type electrical conductivity. In the previously discussed works, the base sensor material was the semiconductor, while the rGO flakes served as conducting channels between the WBS semiconductor structures, enabling more efficient transport of electric charge. The presence of unsaturated bonds on the rGO surface also creates active adsorption centers. Thus, compared to "pure" semiconductors (without rGO flakes) in the WBS + rGO structures, additional active sites are available for anchoring gaseous molecules. The WBS + rGO heterostructure is a random network of semiconductor nanostructures bridged by rGO nanoflakes. The difference of the Fermi levels of the n-type WBS and the p-type rGO may lead to the formation of p–n microjunctions at the phase boundaries. Before exposure to gas, the resistance for both "pure" semiconductor sensors and WBS + rGO heterostructures is mainly influenced by the adsorption of oxygen from the air. The presence of rGO increases the surface area for the adsorption of chemisorbed oxygen and target gas. Usually, the oxygen molecules from the air are adsorbed on the semiconductor surface and at the grain boundaries in the forms of O_2^-, O^- or O^{2-} ions. Next, these ions capture free electric charge from the conduction band of semiconductors that creates a charged area on the sensor surface. The mechanism of NO_2 detection by structure based on a "pure" semiconductor (without rGO flakes) mainly consists in modifying the charged region formed by oxygen after exposure to the gas.

For WBS+rGO heterostructures, the depletion area formed at the inter-grain boundaries between the n-type semiconductor and the p-type rGO also affects the electrical resistance of the sensor structure. The increase in sensor resistance observed after exposure to a gas analyte is due to a change in the concentration of charge carriers in the conduction band, caused by gas molecules adsorbed on the sensor surface. When the sensor is exposed to NO_2 (which is electrophilic in nature), the incident gas molecules capture free electrons directly from the conduction band of the structure and are adsorbed on the surface. Nitrogen present in the NO_2 molecule has one unpaired electron, which promotes the chemisorption of NO_2 molecules at the surface. The large surface offered by semiconductor nanostructures additionally supports the increased adsorption of gas molecules. Since

the electron affinity of NO_2 (2.27 eV) is higher than oxygen (0.45 eV), the absorbed NO_2 molecules interact with the adsorbed oxygen ions and capture their electrons. The flow of electric charge from the surface of the WBS + rGO sensor to the molecules of the detected gas and from the adsorbed oxygen additionally increases the width of the depletion region, which leads to a significant increase in the sensor resistance.

6. Conclusions

Adding rGO to n-type oxide semiconductors, whose surface is negatively charged by electrons from the volume of the semiconductor and by electrons from the surrounding atmosphere located in the interface states with high density, weakens the hybridization of this surface.

Due to the presence of rGO in the semiconductor nanostructures, the interaction of NO_2 with the surface of the semiconductor exhibits more physical nature than chemical, as is observed for the "pure semiconductor". This new situation also causes the interaction of NO_2 with the surface of the semiconductor to be more selective (rGO molecules both limit the amount of negative charge accumulated in the surface states and reduce the intensity of the electric field generated by the electric charge in the interface states). It is also important that rGO molecules form relatively large nanostructures that affect the distribution of the electric field in the area where they are located.

In the case of semiconductor nanostructures obtained by hydrothermal methods, both the shapes of the nanostructures and their sizes and electrical properties (their resistivity) depend on the technology of their production. In the sensor aspect, the optimal rGO concentration for different semiconductors, and for different production technologies, is different. There cannot be too few rGO nanostructures, because they will not sufficiently modify the surface of semiconductor nanostructures (their surface electrical properties). There cannot be too many rGO nanostructures because they will "dominate" the ongoing interactions of semiconductor nanostructures with NO_2; first of all, they will "separate" NO_2 and oxygen molecules too much from semiconductor nanostructures.

The physical-type interaction between semiconductor nanoparticles and NO_2 particles occurs to a greater extent in WBS+rGO structures than in WBS without rGO. This causes semiconductor nanostructures containing rGO to be much easier to detoxify. The process of detoxification does not require elevated temperature and is significantly faster—it takes several or several dozen seconds. The analyses carried out in this paper indicate that the modification of the physicochemical properties of the nanostructures of semiconductors, by the use of rGO nanoflakes, can significantly improve the sensor properties of such structures.

Author Contributions: Conceptualization, S.D. and Ł.D.; validation, S.D. and Ł.D.; writing—original draft preparation, S.D., Ł.D. and T.P.; writing—review and editing, S.D., Ł.D. and T.P.; visualization, Ł.D. and S.D.; supervision, S.D., Ł.D. and T.P. All authors have read and agreed to the published version of the manuscript.

Data Availability Statement: Not applicable.

References

1. Kumunda, C.; Adekunle, A.S.; Mamba, B.B.; Hlongwa, N.W.; Nkambule, T.T.I. Electrochemical Detection of Environmental Pollutants Based on Graphene Derivatives: A Review. *Front. Mater.* **2021**, *7*. [CrossRef]
2. B, G.R.; M, S.B.R.; Kailasa, S.; Maseed, H.; Bikshalu, K.; K, V.R. Comparative gas sensing analysis of green and chemically reduced graphene oxide. *Mater. Res. Express* **2019**, *6*, 115624. [CrossRef]
3. Park, J.; Kim, Y.; Park, S.Y.; Sung, S.J.; Jang, H.W.; Park, C.R. Band gap engineering of graphene oxide for ultrasensitive NO_2 gas sensing. *Carbon* **2019**, *159*, 175–184. [CrossRef]

4. Marcos-Viquez, A.L.; Miranda, A.; Cruz-Irisson, M.; Pérez, L.A. Tin carbide monolayers as potential gas sensors. *Mater. Lett.* **2021**, *294*, 129751. [CrossRef]

5. Gomaa, M.; Sayed, M.; Patil, V.; Boshta, M.; Patil, P. Gas sensing performance of sprayed NiO thin films toward NO_2 gas. *J. Alloy. Compd.* **2021**, *885*, 160908. [CrossRef]

6. World Health Organization, Ambient (outdoor) air pollution. Available online: https://www.who.int/news-room/fact-sheets/detail/ambient-(outdoor)-air-quality-and-health (accessed on 28 May 2022).

7. Yi, N.; Cheng, Z.; Li, H.; Yang, L.; Zhu, J.; Zheng, X.; Chen, Y.; Liu, Z.; Zhu, H.; Cheng, H. Stretchable, ultrasensitive, and low-temperature NO_2 sensors based on MoS2@rGO nanocomposites. *Mater. Today Phys.* **2020**, *15*, 100265. [CrossRef]

8. Wu, J.; Wu, Z.; Ding, H.; Wei, Y.; Huang, W.; Yang, X.; Li, Z.; Qiu, L.; Wang, X. Flexible, 3D SnS_2/Reduced graphene oxide heterostructured NO_2 sensor. *Sensors Actuators B Chem.* **2019**, *305*, 127445. [CrossRef]

9. Ganapathi, K.; Kaur, M.; Shaheera, M.; Pathak, A.; Gadkari, S.; Debnath, A. Highly sensitive NO_2 sensor based on ZnO nanostructured thin film prepared by SILAR technique. *Sensors Actuators B Chem.* **2021**, *335*, 129678. [CrossRef]

10. Procek, M.; Pustelny, T.; Stolarczyk, A. Influence of External Gaseous Environments on the Electrical Properties of ZnO Nanostructures Obtained by a Hydrothermal Method. *Nanomaterials* **2016**, *6*, 227. [CrossRef]

11. Khudadad, A.I.; Yousif, A.A.; Abed, H.R. Effect of heat treatment on WO3 nanostructures based NO_2 gas sensor low-cost device. *Mater. Chem. Phys.* **2021**, *269*, 124731. [CrossRef]

12. Zhou, L.; Hu, Z.; Wang, P.; Gao, N.; Zhai, B.; Ouyang, M.; Zhang, G.; Chen, B.; Luo, J.; Jiang, S.; et al. Enhanced NO_2 sensitivity of SnO_2 SAW gas sensors by facet engineering. *Sensors Actuators B: Chem.* **2022**, *361*, 131735. [CrossRef]

13. Sangale, S.S.; Jadhav, V.V.; Shaikh, S.F.; Shinde, P.V.; Ghule, B.G.; Raut, S.D.; Tamboli, M.S.; Al-Enizi, A.M.; Mane, R.S. Facile one-step hydrothermal synthesis and room-temperature NO_2 sensing application of α-Fe_2O_3 sensor. *Mater. Chem. Phys.* **2020**, *246*, 122799. [CrossRef]

14. Pustelny, T.; Ignac-Nowicka, J.; Opilski, Z. Optical investigations on layered methalphthalicyanine nanostructures affected by NO2 applying the surface plasmon resonance method. *Opt. Appl.* **2004**, *34*, 563–572.

15. Pustelny, T.; Setkiewicz, M.; Drewniak, S.; Maciak, E.; Stolarczyk, A.; Urbańczyk, M.; Procek, M.; Gut, K.; Opilski, Z.; Pasternak, I.; et al. The sensibility of resistance sensor structures with graphene to the action of selected gaseous media. *Bull. Pol. Acad. Sci. Tech. Sci.* **2013**, *61*, 293–300. [CrossRef]

16. Han, T.; Gao, S.; Wang, Z.; Fei, T.; Liu, S.; Zhang, T. Investigation of the effect of oxygen-containing groups on reduced graphene oxide-based room-temperature NO_2 sensor. *J. Alloy. Compd.* **2019**, *801*, 142–150. [CrossRef]

17. Guo, L.; Hao, Y.-W.; Li, P.-L.; Song, J.-F.; Yang, R.-Z.; Fu, X.-Y.; Xie, S.-Y.; Zhao, J.; Zhang, Y.-L. Improved NO2 Gas Sensing Properties of Graphene Oxide Reduced by Two-beam-laser Interference. *Sci. Rep.* **2018**, *8*, 1–7. [CrossRef] [PubMed]

18. Black, N.; Liu, C.; Pearce, R.; Li, B.; Maier, S.; Cohen, L.; Gallop, J.; Hao, L. Graphene gas sensing using a non-contact microwave method. *Nanotechnology* **2017**, *28*, 395501. [CrossRef]

19. Hu, H.; Yang, X.; Guo, X.; Khaliji, K.; Biswas, S.R.; De Abajo, F.J.G.; Low, T.; Sun, Z.; Dai, Q. Gas identification with graphene plasmons. *Nat. Commun.* **2019**, *10*, 1–7. [CrossRef]

20. Majhi, S.; Mirzaei, A.; Kim, H.; Kim, S. Reduced Graphene Oxide (rGO)-Loaded Metal-Oxide Nanofiber Gas Sensors: An Overview. *Sensors* **2021**, *21*, 1352. [CrossRef]

21. Armano, A.; Agnello, S. Two-Dimensional Carbon: A Review of Synthesis Methods, and Electronic, Optical, and Vibrational Properties of Single-Layer Graphene. *C* **2019**, *5*, 67. [CrossRef]

22. Sur, U.K. Graphene: A Rising Star on the Horizon of Materials Science. *Int. J. Electrochem.* **2012**, *2012*, 1–12. [CrossRef]

23. Pisarkiewicz, T.; Maziarz, W.; Małolepszy, A.; Stobiński, L.; Michoń, D.; Rydosz, A. Multilayer Structure of Reduced Graphene Oxide and Copper Oxide as a Gas Sensor. *Coatings* **2020**, *10*, 1015. [CrossRef]

24. Chatterjee, S.G.; Chatterjee, S.; Ray, A.K.; Chakraborty, A.K. Graphene–metal oxide nanohybrids for toxic gas sensor: A review. *Sensors Actuators B: Chem.* **2015**, *221*, 1170–1181. [CrossRef]

25. Rowley-Neale, S.J.; Randviir, E.P.; Dena, A.S.A.; Banks, C.E. An overview of recent applications of reduced graphene oxide as a basis of electroanalytical sensing platforms. *Appl. Mater. Today* **2018**, *10*, 218–226. [CrossRef]

26. Łukowiec, D.; Kubacki, J.; Kałużyński, P.; Procek, M.; Wacławek, S.; Radoń, A. Formation and role in gas sensing properties of spherical and hollow silver nanoparticles deposited on the surface of electrochemically exfoliated graphite. *Appl. Surf. Sci.* **2021**, *580*, 152316. [CrossRef]

27. Drewniak, S.; Pustelny, T.; Muzyka, R.; Stolarczyk, A.; Konieczny, G. Investigations of selected physical properties of graphite oxide and thermally exfoliated/reduced graphene oxide in the aspect of their applications in photonic gas sensors. *Photon- Lett. Pol.* **2015**, *7*, 2. [CrossRef]

28. Wu, T.-C.; Dai, J.; Hu, G.; Yu, W.-B.; Ogbeide, O.; De Luca, A.; Huang, X.; Su, B.-L.; Li, Y.; Udrea, F.; et al. Machine-intelligent inkjet-printed α-Fe_2O_3/rGO towards NO_2 quantification in ambient humidity. *Sensors Actuators B: Chem.* **2020**, *321*, 128446. [CrossRef]

29. Pei, S.; Cheng, H.-M. The reduction of graphene oxide. *Carbon* **2012**, *50*, 3210–3228. [CrossRef]

30. Stobinski, L.; Lesiak, B.; Malolepszy, A.; Mazurkiewicz, M.; Mierzwa, B.; Zemek, J.; Jiricek, P.; Bieloshapka, I. Graphene oxide and reduced graphene oxide studied by the XRD, TEM and electron spectroscopy methods. *J. Electron Spectrosc. Relat. Phenom.* **2014**, *195*, 145–154. [CrossRef]

31. Drewniak, S.; Muzyka, R.; Stolarczyk, A.; Pustelny, T.; Kotyczka-Morańska, M.; Setkiewicz, M. Studies of Reduced Graphene Oxide and Graphite Oxide in the Aspect of Their Possible Application in Gas Sensors. *Sensors* **2016**, *16*, 103. [CrossRef]

32. Botas, C.; Álvarez, P.; Blanco, C.; Santamaria, R.; Granda, M.; Gutiérrez, M.D.; Rodriguez-Reinoso, F.; Menéndez, R. Critical temperatures in the synthesis of graphene-like materials by thermal exfoliation–reduction of graphite oxide. *Carbon* **2013**, *52*, 476–485. [CrossRef]

33. Muzyka, R.; Drewniak, S.; Pustelny, T.; Chrubasik, M.; Gryglewicz, G. Characterization of Graphite Oxide and Reduced Graphene Oxide Obtained from Different Graphite Precursors and Oxidized by Different Methods Using Raman Spectroscopy. *Materials* **2018**, *11*, 1050. [CrossRef] [PubMed]

34. Drewniak, S.; Procek, M.; Muzyka, R.; Pustelny, T. Comparison of Gas Sensing Properties of Reduced Graphene Oxide Obtained by Two Different Methods. *Sensors* **2020**, *20*, 3175. [CrossRef]

35. Imae, I. Reduction of Graphene Oxide Using an Environmentally Friendly Method and Its Application to Energy-Related Materials. *Coatings* **2021**, *11*, 297. [CrossRef]

36. Sali, S.; Mackey, H.R.; Abdala, A.A. Effect of Graphene Oxide Synthesis Method on Properties and Performance of Polysulfone-Graphene Oxide Mixed Matrix Membranes. *Nanomaterials* **2019**, *9*, 769. [CrossRef] [PubMed]

37. Tarcan, R.; Todor-Boer, O.; Petrovai, I.; Leordean, C.; Astilean, S.; Botiz, I. Reduced graphene oxide today. *J. Mater. Chem. C* **2019**, *8*, 1198–1224. [CrossRef]

38. Lawal, A.T. Graphene-based nano composites and their applications. A review. Biosens. *Bioelectron.* **2019**, *141*, 111384. [CrossRef]

39. Bonavolontà, C.; Vettoliere, A.; Falco, G.; Aramo, C.; Rendina, I.; Ruggiero, B.; Silvestrini, P.; Valentino, M. Reduced graphene oxide on silicon-based structure as novel broadband photodetector. *Sci. Rep.* **2021**, *11*, 1–10. [CrossRef]

40. Sieradzka, M.; Ślusarczyk, C.; Biniaś, W.; Fryczkowski, R. The Role of the Oxidation and Reduction Parameters on the Properties of the Reduced Graphene Oxide. *Coatings* **2021**, *11*, 166. [CrossRef]

41. Osmieri, L.; Videla, A.H.A.M.; Specchia, S. The use of different types of reduced graphene oxide in the preparation of Fe-N-C electrocatalysts: Capacitive behavior and oxygen reduction reaction activity in alkaline medium. *J. Solid State Electrochem.* **2016**, *20*, 3507–3523. [CrossRef]

42. Loryuenyong, V.; Totepvimarn, K.; Eimburanapravat, P.; Boonchompoo, W.; Buasri, A. Preparation and Characterization of Reduced Graphene Oxide Sheets via Water-Based Exfoliation and Reduction Methods. *Adv. Mater. Sci. Eng.* **2013**, *2013*, 923403. [CrossRef]

43. Bing, C.; Jiahao, Y.; Xiaoying, L.; Qi, J.; Guoping, W.; Linghua, J. Effects of reduction method on reduced graphene oxide and its electrochemical energy storage performance. *Diam. Relat. Mater.* **2021**, *114*, 108305. [CrossRef]

44. Spilarewicz-Stanek, K.; Kisielewska, A.; Ginter, J.; Bałuszyńska, K.; Piwoński, I. Elucidation of the function of oxygen moieties on graphene oxide and reduced graphene oxide in the nucleation and growth of silver nanoparticles. *RSC Adv.* **2016**, *6*, 60056–60067. [CrossRef]

45. Lesiak, B.; Trykowski, G.; Tóth, J.; Biniak, S.; Kövér, L.; Rangam, N.; Stobinski, L.; Malolepszy, A. Chemical and structural properties of reduced graphene oxide—dependence on the reducing agent. *J. Mater. Sci.* **2020**, *56*, 3738–3754. [CrossRef]

46. Gao, H.; Ma, Y.; Song, P.; Leng, J.; Wang, Q. Gas sensor based on rGO/ZnO aerogel for efficient detection of NO_2 at room temperature. *J. Mater. Sci. Mater. Electron.* **2021**, *32*, 10058–10069. [CrossRef]

47. Zhu, X.; Zhou, Y.; Guo, Y.; Ren, H.; Gao, C. Nitrogen dioxide sensing based on multiple-morphology cuprous oxide mixed structures anchored on reduced graphene oxide nanosheets at room temperature. *Nanotechnology* **2019**, *30*, 455502. [CrossRef]

48. Zhang, H.; Yu, L.; Li, Q.; Du, Y.; Ruan, S. Reduced graphene oxide/α-Fe_2O_3 hybrid nanocomposites for room temperature NO_2 sensing. *Sensors Actuators B: Chem.* **2017**, *241*, 109–115. [CrossRef]

49. Cheng, M.; Wu, Z.; Liu, G.; Zhao, L.; Gao, Y.; Zhang, B.; Liu, F.; Yan, X.; Liang, X.; Sun, P.; et al. Highly sensitive sensors based on quasi-2D rGO/SnS_2 hybrid for rapid detection of NO_2 gas. *Sensors Actuators B: Chem.* **2019**, *291*, 216–225. [CrossRef]

50. Sivakumar, R.; Krishnamoorthi, K.; Vadivel, S.; Govindasamy, S. Progress towards a novel NO_2 gas sensor based on SnO_2/RGO hybrid sensors by a facial hydrothermal approach. *Diam. Relat. Mater.* **2021**, *116*, 108418. [CrossRef]

51. Rigoletto, M.; Calza, P.; Gaggero, E.; Laurenti, E. Hybrid materials for the removal of emerging pollutants in water: Classification, synthesis, and properties. *Chem. Eng. J. Adv.* **2022**, 10. [CrossRef]

52. Choudhari, A.; Bhanvase, B.A.; Saharan, V.K.; Salame, P.; Hunge, Y. Sonochemical preparation and characterization of rGO/SnO_2 nanocomposite: Electrochemical and gas sensing performance. *Ceram. Int.* **2020**, *46*, 11290–11296. [CrossRef]

53. Li, L.; He, S.; Liu, M.; Zhang, C.; Chen, W. Three-Dimensional Mesoporous Graphene Aerogel-Supported SnO_2 Nanocrystals for High-Performance NO_2 Gas Sensing at Low Temperature. *Anal. Chem.* **2015**, *87*, 1638–1645. [CrossRef] [PubMed]

54. Du, H.; Xie, G.; Zhang, Q. Enhanced Room Temperature NO_2 Sensing Performance of RGO Nanosheets by Building RGO/SnO_2 Nanocomposite System. *Sensors* **2019**, *19*, 4650. [CrossRef] [PubMed]

55. Wang, X.; Marikutsa, A.V.; Rumyantseva, M.N.; Gaskov, A.; Knotko, A.; Li, X. p-n Transition-Enhanced Sensing Properties at Room Temperature. *IEEE Sens. J.* **2020**, *20*, 4562–4570. [CrossRef]

56. Li, G.; Shen, Y.; Zhou, P.; Hao, F.; Fang, P.; Wei, D.; Meng, D.; San, X. Design and application of highly responsive and selective rGO-SnO_2 nanocomposites for NO_2 monitoring. *Mater. Charact.* **2020**, *163*, 110284. [CrossRef]

57. Wang, Y.; Liu, L.; Sun, F.; Li, T.; Zhang, T.; Qin, S. Humidity-Insensitive NO_2 Sensors Based on SnO_2/rGO Composites. *Front. Chem.* **2021**, *9*, 681313. [CrossRef]

58. Wu, L.; Shao, H.; Yang, C.; Feng, X.; Han, L.; Zhou, Y.; Du, W.; Sun, X.; Xu, Z.; Zhang, X.; et al. SnS2 Nanosheets with RGO Modification as High-Performance Anode Materials for Na-Ion and K-Ion Batteries. *Nanomaterials* **2021**, *11*, 1932. [CrossRef]

59. Shafiei, M.; Bradford, J.; Khan, H.; Piloto, C.; Wlodarski, W.; Li, Y.; Motta, N. Low-operating temperature NO₂ gas sensors based on hybrid two-dimensional SnS₂-reduced graphene oxide. *Appl. Surf. Sci.* **2018**, *462*, 330–336. [CrossRef]

60. Liu, S.; Yu, B.; Zhang, H.; Fei, T.; Zhang, T. Enhancing NO₂ gas sensing performances at room temperature based on reduced graphene oxide-ZnO nanoparticles hybrids. *Sensors Actuators B: Chem.* **2014**, *202*, 272–278. [CrossRef]

61. Bai, S.; Han, J.; Meng, J.C.; Sun, L.; Sun, J.; Zhao, Y.; Tang, P.; Luo, R.; Li, D.; Chen, A. NiO/ZnO composite decorated on rGO for detection of NO₂. *Sensors Actuators B: Chem.* **2021**, *339*, 129720. [CrossRef]

62. Gao, R.; Gao, L.; Zhang, X.; Gao, S.; Xu, Y.; Cheng, X.; Guo, G.; Ye, Q.; Zhou, X.; Major, Z.; et al. The controllable assembly of the heterojunction interface of the ZnO@rGO for enhancing the sensing performance of NO₂ at room temperature and sensing mechanism. *Sensors Actuators B: Chem.* **2021**, *342*, 130073. [CrossRef]

63. Galstyan, V.; Comini, E.; Kholmanov, I.; Ponzoni, A.; Sberveglieri, V.; Poli, N.; Faglia, G.; Sberveglieri, G. Graphene-zinc Oxide Based Nanomaterials for Gas Sensing Devices. *Procedia Eng.* **2016**, *168*, 1172–1175. [CrossRef]

64. Geng, X.; Zhang, C.; Olivier, M.-G.; Debliquy, M. Room Temperature NO2 Responses of Visible-Light Activated Nanosheet rGO@ZnO1−x Sensors. *Proceedings* **2017**, *1*, 411. [CrossRef]

65. Ngo, Y.-L.T.; Hur, S.H. Low-temperature NO₂ gas sensor fabricated with NiO and reduced graphene oxide hybrid structure. *Mater. Res. Bull.* **2016**, *84*, 168–176. [CrossRef]

66. Liang, Y.-C.; Chang, Y.-C.; Zhao, W.-C. Design and Synthesis of Novel 2D Porous Zinc Oxide-Nickel Oxide Composite Nanosheets for Detecting Ethanol Vapor. *Nanomaterials* **2020**, *10*, 1989. [CrossRef]

67. Pisarkiewicz, T.; Maziarz, W.; Małolepszy, A.; Stobiński, L.; Michoń, D.A.; Szkudlarek, A.; Pisarek, M.; Kanak, J.; Rydosz, A. Nitrogen Dioxide Sensing using Multilayer Structure of Reduced Graphene Oxide and α-Fe₂O₃. *Sensors* **2021**, *21*, 1011. [CrossRef]

68. Tang, X.; Tian, C.; Zou, C. Highly sensitive and selective room-temperature NO₂ gas sensor based on novel Fe2O3 nanorings/reduced graphene oxide heterojunction nanocomposites. *Optik* **2021**, *241*, 166951. [CrossRef]

69. Huang, M.; Wang, Y.; Ying, S.; Wu, Z.; Liu, W.; Chen, D.; Peng, C. Synthesis of Cu₂O-Modified Reduced Graphene Oxide for NO₂ Sensors. *Sensors* **2021**, *21*, 1958. [CrossRef]

70. Nia, P.M.; Meng, W.P.; Lorestani, F.; Mahmoudian, M.; Alias, Y. Electrodeposition of copper oxide/polypyrrole/reduced graphene oxide as a nonenzymatic glucose biosensor. *Sensors Actuators B: Chem.* **2015**, *209*, 100–108. [CrossRef]

71. Meng, H.; Yang, W.; Ding, K.; Feng, L.; Guan, Y. Cu₂O nanorods modified by reduced graphene oxide for NH3 sensing at room temperature. *J. Mater. Chem. A* **2014**, *3*, 1174–1181. [CrossRef]

72. Wang, L.; Zhang, R.; Zhou, T.; Lou, Z.; Deng, J.; Zhang, T. Concave Cu₂O octahedral nanoparticles as an advanced sensing material for benzene (C₆H₆) and nitrogen dioxide (NO₂) detection. *Sensors Actuators B: Chem.* **2015**, *223*, 311–317. [CrossRef]

73. Shen, Y.; Tian, F.H.; Chen, S.; Ma, Z.; Zhao, L.; Jia, X. Density functional theory study on the mechanism of CO sensing on Cu₂O (111) surface: Influence of the pre-adsorbed oxygen atom. *Appl. Surf. Sci.* **2014**, *288*, 452–457. [CrossRef]

74. Pan, J.; Liu, W.; Quan, L.; Han, N.; Bai, S.; Luo, R.; Feng, Y.; Li, D.; Chen, A. Cu2O and rGO Hybridizing for Enhancement of Low-Concentration NO2 Sensing at Room Temperature. *Ind. Eng. Chem. Res.* **2018**, *57*, 10086–10094. [CrossRef]

75. Wan, X.; Wang, J.; Zhu, L.; Tang, J. Gas sensing properties of Cu2O and its particle size and morphology-dependent gas-detection sensitivity. *J. Mater. Chem. A* **2014**, *2*, 13641–13647. [CrossRef]

76. Steinhauer, S. Gas Sensors Based on Copper Oxide Nanomaterials: A Review. *Chemosensors* **2021**, *9*, 51. [CrossRef]